JCTC Journal of Chemical Theory and Computation

Article

pubs.acs.org/JCTC

# Influence of Grid Spacing in Poisson−Boltzmann Equation Binding Energy Estimation

Robert C. Harris,[‡] Alexander H. Boschitsch,[§] and Marcia O. Fenley*[,†]

[†]Institute of Molecular Biophysics and [‡]Department of Physics, Florida State University, Tallahasse, Florida 32306, United States

[§]Continuum-Dynamics Inc., 34 Lexington Avenue, Ewing, New Jersey 08618, United States

**ABSTRACT:** Grid-based solvers of the Poisson−Boltzmann, PB, equation are routinely used to estimate electrostatic binding, $\Delta\Delta G_{el}$, and solvation, $\Delta G_{el}$, free energies. The accuracies of such estimates are subject to grid discretization errors from the finite difference approximation to the PB equation. Here, we show that the grid discretization errors in $\Delta\Delta G_{el}$ are more significant than those in $\Delta G_{el}$, and can be divided into two parts: (i) errors associated with the relative positioning of the grid and (ii) systematic errors associated with grid spacing. The systematic error in particular is significant for methods, such as the molecular mechanics PB surface area (MM-PBSA) approach, that predict electrostatic binding free energies by averaging over an ensemble of molecular conformations. Although averaging over multiple conformations can control for the error associated with grid placement, it will not eliminate the systematic error, which can only be controlled by reducing grid spacing. The present study indicates that the widely used grid spacing of 0.5 Å produces unacceptable errors in $\Delta\Delta G_{el}$, even though its predictions of $\Delta G_{el}$ are adequate for the cases considered here. Although both grid discretization errors generally increase with grid spacing, the relative sizes of these errors differ according to the solute−solvent dielectric boundary definition. The grid discretization errors are generally smaller on the Gaussian surface used in the present study than on either the solvent-excluded or the van der Waals surfaces, which both contain more surface discontinuities (e.g., sharp edges and cusps). Additionally, all three molecular surfaces converge to very different estimates of $\Delta\Delta G_{el}$.

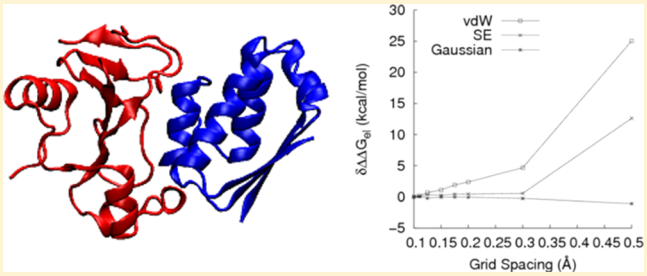


## INTRODUCTION

Many cellular processes, such as signal transduction, gene expression, and protein synthesis, are governed by the binding of biomolecules. In pharmaceutical applications, accurate and fast predictions of the binding free energy, $\Delta\Delta G$, of drugs to biomolecular targets, such as proteins and nucleic acids, are necessary, particularly in the final stages of the structure-based drug discovery. Predicting $\Delta\Delta G$ accurately is, however, challenging because it usually involves combining several energies, each of which is subject to numerical and model errors. Some of these energy terms, such as the Coulombic interactions between binding partners, usually favor binding, while others, such as the desolvation penalty of removing charged residues from the solvent environment upon binding, oppose it. Frequently, $\Delta\Delta G$ is much smaller than the contributing energy terms, so that errors judged small when compared against these individual contributions assume much greater significance when estimating $\Delta\Delta G$.

The present study illustrates this general problem by examining the numerical computation of the electrostatic component, $\Delta\Delta G_{el}$, of $\Delta\Delta G$, estimated by the Poisson−Boltzmann, PB, equation.[1−7] Typically, one obtains $\Delta\Delta G_{el}$ from $\Delta\Delta G_{el} = (\Delta G_{el})_c - (\Delta G_{el})_1 - (\Delta G_{el})_2 + (\Delta\Delta G_{el})_{coulomb}$, where $(\Delta G_{el})_c$ is the electrostatic solvation free energy of the complex, $(\Delta G_{el})_1$ and $(\Delta G_{el})_2$ are the corresponding electrostatic solvation free energies of the unbound components, and $(\Delta\Delta G_{el})_{coulomb}$ is the electrostatic binding free energy of the two components in vacuum. Here we assume that there are no conformational changes upon binding and thus, the bound and unbound states of the binding partners are the same. This same assumption is made in the most popular single trajectory MM-PBSA protocol, where only a single all-atom molecular dynamics of the complex is performed to compute $\Delta\Delta G$. Many studies assume that the differences in $\Delta\Delta G$ between closely related complexes, such as the binding of similarly charged organic drugs to a single protein or nucleic acid target or the mutation of polar or charged side chains in protein−ligand complexes, are dominated by the change in $\Delta\Delta G_{el}$.[8,9] However, many of these studies have used grid spacings of 0.5 Å or larger under the justification that $\Delta G_{el}$ estimates computed with these grid spacings are consistent with free energy methods using explicit solvent molecular dynamics simulations[10] or experimental solvation free energy data.[11] As demonstrated below, however, such coarse grids produce estimates of $\Delta\Delta G_{el}$ with unacceptably large errors because the magnitude of $\Delta\Delta G_{el}$ is typically orders of magnitude smaller than $(\Delta G_{el})_1$, $(\Delta G_{el})_2$, and $(\Delta G_{el})_c$.

Finite difference estimates of $\Delta\Delta G_{el}$ by the PB equation contain two kinds of numerical grid discretization error. The

**Received:** September 3, 2012
**Published:** June 14, 2013

   dx.doi.org/10.1021/ct300765w | J. Chem. Theory Comput. 2013, 9, 3677−3685

first error, denoted by $\sigma_{GP}$, is the variation in $\Delta\Delta G_{el}$ due to grid positioning. This error increases with increasing grid spacing but can be controlled by averaging over different grid placements, as described in the Methods section, or through averaging over many similar molecular conformations from a molecular dynamics trajectory, as done in molecular mechanics PB surface area, MM-PBSA, methods.[12] However, these estimates of $\Delta\Delta G_{el}$ also contain a second, systematic error associated with grid spacing that is not eliminated by this averaging. For example, if the estimate of $\Delta\Delta G_{el}$ obtained by averaging over grid positions is denoted by $\langle\Delta\Delta G_{el}\rangle$ then $\langle\Delta\Delta G_{el}\rangle$ obtained at a 1.0 Å grid spacing can differ by more than 100 kcal/mol from that obtained using a 0.3 Å grid size, as shown in the Results section. This error persists when averaging over multiple grid placements and can only be reduced by using finer grid spacing. For the solvent-excluded, SE, and van der Waal's, vdW, surface definitions, the Results confirm that the popular 0.5 Å grid spacing is too coarse for many applications. Recommending a single universally useful grid spacing is difficult because of the innate dependence upon the system considered, surface definition, and energy accuracy required by the application. Rather, users of PBE solvers are urged to perform calculations at multiple grid spacings to ensure that their calculations have converged.

One possibility explored in this study is that the grid convergence behavior of $\langle\Delta\Delta G_{el}\rangle$ is linked to the smoothness of the molecular surface. In the Results, when a smooth Gaussian surface definition,[13] which contained fewer slope discontinuities than either the SE surface, which contains sharp cusps, cones, and convex edges, or the vdW surface, which contains reentrant edges, was used, $\langle\Delta\Delta G_{el}\rangle$ was better converged at larger grid spacings. The better numerical performance of the Gaussian surface does not necessarily imply that it should be used for PB applications.

As shown below, the three molecular surface choices converge to very different estimates of $\Delta\Delta G_{el}$ and, because the ability to predict changes in $\Delta\Delta G$ is the true test of a surface definition, more work will need to be done to determine which surface definition produces results that agree with experiment. While we do not settle this particular issue here, regardless of which surface definition is adopted, the errors associated with grid spacing will need to be accounted for to ensure that reliable estimates of $\Delta\Delta G_{el}$ are procured.

## METHODS

**Data Sets.** Three sets of biomolecular complexes were used in this investigation:

*Data Set 1.* A collection of DNA-minor groove drug complexes whose experimentally determined $\Delta\Delta G$ span a narrow range, thus increasing the challenge of predicting rank orderings. This data set typifies the calculations required in structure-based drug design. The pdbids for Data Set 1 are as follows: 102d, 109d, 121d, 127d, 129d, 166d, 195d, 1d30, 1d63, 1d64, 1d86, 1dne, 1eel, 1fmq, 1fms, 1jtl, 1lex, 1prp, 227d, 261d, 164d, 289d, 298d, 2dbe, 302d, 311d, 328d, and 360d.

*Data Set 2.* Various wild-type and mutant barnase-barstar complexes were included in this study as examples of the common use of in silico mutagenesis in biophysical applications where the goal is to identify residues that make significant contributions to the total binding free energy. The structural data for all mutated complexes were available, so the effects of mutations on the three-dimensional structure can be considered without further molecular modeling. The pdbids for Data Set 2 are as follows: 1b27, 1b2s, 1b2u, 1b3s, 2aza4, 1x1w, 1x1y, 1x1u, and 1x1x.

*Data Set 3.* RNA-peptide complexes with various biological functions, RNA folds, peptide secondary structures and binding affinities. The pdbids for Data Set 3 are as follows: 1a1t, 1a4t, 1biv, 1exy, 1g70, 1hji, 1i9f, 1mnb, 1nyb, 1qfq, 1ull, 1zbn, 2a9x, and 484d.

**Structure Preparation.** The atomic coordinate files (pdb files) of all biomolecular complexes in this study were taken from the Research Collaboratory for Structural Bioinformatics (RCSB) database.[14] For the NMR structures model 1 was used. Only the chains containing the drug, nucleic acid, or protein were retained while all other unnecessary information was removed prior to further manipulation of the pdb files. For Data Set 1 the molecular modeling protocol used to create the pqr files was described elsewhere.[15] For the other two data sets the pdb2pqr program[16] was used to prepare the pqr files, which contained the atomic coordinates, as well as atomic partial charges and van der Waals radii, assigned according to the Amber[17] force field for proteins and nucleic acids. All ionizable protein residues were left in their standard ionization states at pH = 7, with the histidine side chains left neutral. For the hydrogen atoms that had a zero radius, the atomic radius was taken as that of the smallest one (0.6 Å) in the Amber force field. However, these changes in atomic radii did not change the results presented here because each of these hydrogen atoms is contained well inside another atom with finite radius (results not shown). The pqr files used in this work can be downloaded from http://www.sb.fsu.edu/~mfenley/convergence/downloads/convergence_pqr_sets.tar.gz.

**Poisson–Boltzmann Calculation Details.** All results were obtained with the adaptive Cartesian grid (ACG) finite difference Poisson–Boltzmann equation solver described elsewhere.[3] This software solves the PB equation and determines the electrostatic potential on an octree structure consisting of hierarchically nested cubes, as shown in Figure 1. The hierarchical grid structure provides a variable mesh spacing capability together with an efficient means of implementing a multigrid solution scheme. In addition, the potential field is decomposed so that singularities are eliminated from the numerical solution. Specifically, inside the molecule the reaction field potential is computed, while outside the molecule the full potential is obtained. At the dielectric interface, the solutions are coupled together using the Coulombic potential, which is easily evaluated analytically. The reaction field generally varies most rapidly at the surface and becomes smooth as one moves deeper into the molecule. Similarly the full potential field calculated outside the molecule also varies most rapidly at surfaces and becomes increasingly smooth farther away. Consequently, the finest mesh spacing requirements occur near the dielectric interface. Elsewhere, coarse grid spacing is permitted, leading to substantial reductions in the overall number of grid points (and thus memory and computation time requirements) needed to compute the solution.

Three molecular surface definitions are considered here: the SE surface, the vdW surface, and a Gaussian surface definition. In the vdW surface definition, a molecule is represented by a union of spheres, one for each atom, centered at the coordinates of that atom in the structure file and the vdW radius of the atom. The molecular surface then consists of the nonoverlapping regions of the surfaces of these spheres. As shown in Figure 2, the vdW surface contains numerous

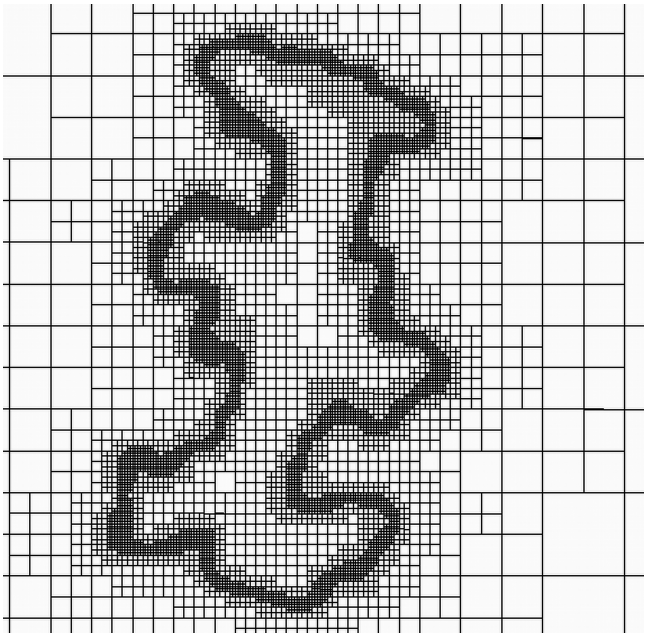

**Figure 1.** Cut through the adaptive Cartesian grid around the B-DNA dodecamer that binds to the cationic propamidine drug (pdbid: 102d) and the surrounding high-dielectric solvent region. Note that the ACG concentrates grid points at the dielectric interface where both the interior reaction field potential and the exterior full potential solutions vary most rapidly. Deeper inside the molecule and further outside it these solutions vary more gradually, so coarser grids can be used.

reentrant edges coinciding with the sphere intersection arcs and characterized by slope discontinuities. The SE surface defines the molecular interior as the region that cannot be covered by a solvent-sized spherical probe (here taken to have a radius of 1.4 Å) without the probe overlapping the interior of the molecule defined by the vdW surface. This definition eliminates the reentrant edges, but introduces cusps and convex edges pointing into the exterior region where the solvent probe intersects itself (i.e., can approach the surface from different directions) as observed from Figure 2. Generally, the SE surface has fewer locations with slope discontinuities than the vdW surface, and the geometries of the discontinuities are different. These factors are known to affect the local behaviors of the potential field and can give rise to singular electric fields (potential gradients). It is not unreasonable to suppose that the number and nature of surface slope discontinuities also affects binding energy predictions is therefore not unreasonable. Finally, the Gaussian surface[13] is implicitly defined by $F(\mathbf{r}) = 0$, where

$$F(\mathbf{r}) = \sum \exp(-|\mathbf{r} - \boldsymbol{\rho}_i|^2/\alpha \mathbf{a}_i^2) - \exp(-1/\alpha) \quad (1)$$

where $\mathbf{r}$ is the evaluation point, $\boldsymbol{\rho}_i$ and $\mathbf{a}_i$ are the atomic centers and radii, respectively, $\alpha$ is the smoothing parameter, and the summation is taken over all atoms. Unless otherwise stated, the results presented here used $\alpha = 1.4$. Note that for a single sphere the Gaussian, SE, and vdW definitions all coincide. Note too that the dielectric constant in the Gaussian surface used in this study does not vary gradually at the molecular surface (as in the PBE solver, ZAP[18]). Instead, the surface where $F(\mathbf{r}) = 0$ forms a sharp demarcation between the interior and exterior dielectric regions. The Gaussian surface generally contains no slope discontinuities, though regions with high curvature can occasionally arise. These regions become more pronounced as $\alpha$ approaches zero and the Gaussian surface converges to the vdW surface. All three surface definitions can contain cavities or regions within the molecule that do not connect with points in the exterior. Per the surface definitions above, these cavities are assigned an exterior dielectric constant in this study.

All of the surface definitions are processed analytically within the ACG PBE solver. No reference to an externally generated triangulated surface is made.

The temperature of the ionic solution was 298.15 K, the dielectric constants for solute and solvent were 1 and 80, and the ionic strength was 100 mM NaCl. No ion-exclusion region was considered in this study. All of the calculations in this study

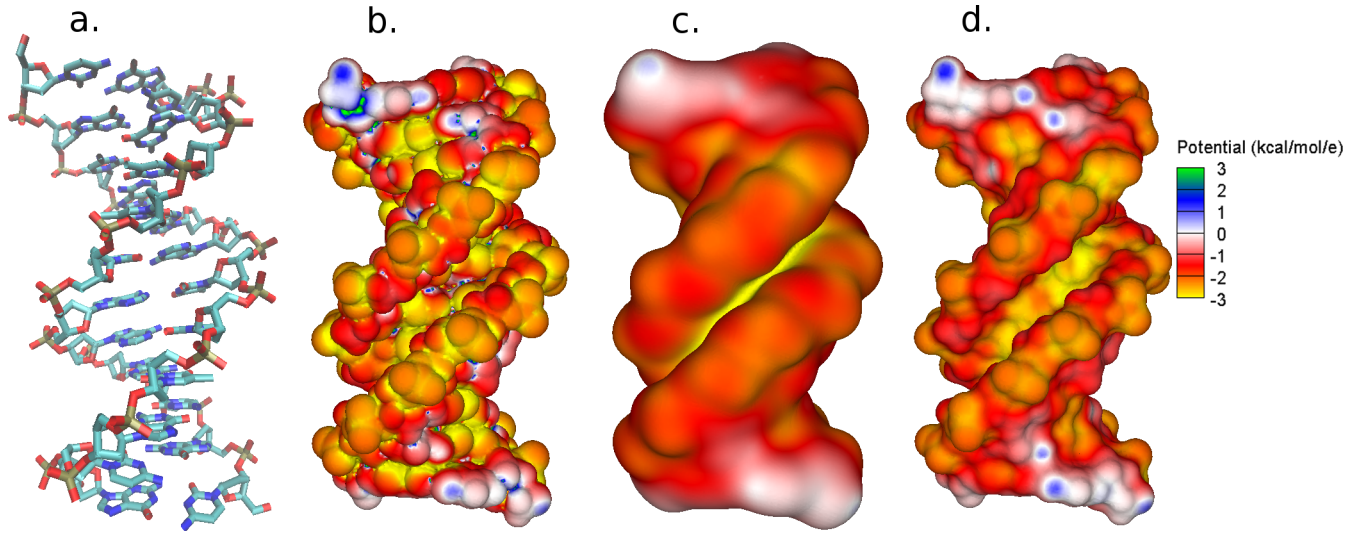


**Figure 2.** Comparison of the surface electrostatic potential on a B-DNA dodecamer (pdbid: 102d) using different molecular surfaces to specify the solute−solvent dielectric boundary. (a) A licorice representation of the B-DNA, with the phosphorus atom of the phosphate group colored yellow. (b−d) The electrostatic potentials on the van der Waals surface, the Gaussian surface ($\alpha = 1.4$), and the solvent-excluded surface, respectively. The electrostatic potentials are displayed in units of kcal/mol/e, and the scale is shown in the figure. The cationic propamidine drug binds in the AT-rich and narrow minor groove of the B-DNA, which displays a pronounced negative potential, but this drug is not shown in this figure.

used the linear PB equation, but nonlinear PB results did not differ significantly from those presented here (data not shown). The finite-difference equations were iteratively solved until the change in dimensionless potential at any grid point was less than $10^{-9}$, which typically occurred within at most 200 multigrid iterations. The total grid size was set to 3 times the largest dimension of the solute, and the outer boundary conditions were assigned using charge conservation principles as described elsewhere.[2] Grids with common dimensions and alignments were generated for each separate binding partner and complex. The ACG predictions of $\Delta G_{el}$ and $\Delta\Delta G_{el}$ were corroborated by similar computations with APBS[19] and an in-house stochastic linear PB solver[5−7] (results not shown).

To quantify the error, $\sigma_{GP}$, due to grid placement, $\Delta\Delta G_{el}$ was computed on 30 different grids generated by shifting the original grid by a uniformly distributed fraction of a grid spacing in each of the $x$, $y$, and $z$ directions. The average ($\langle\Delta\Delta G_{el}\rangle$) and standard deviations ($\sigma_{GP}$) of these energies at each grid spacing are reported in Results.

## RESULTS AND DISCUSSION

**Examining the Convergence of $\Delta\Delta G_{el}$ for Biomolecules.** A grid spacing of 0.5 Å is often used to predict $\Delta\Delta G_{el}$ because experience[20,21] has shown that it generates seemingly well-converged estimates of $\Delta G_{el}$, as shown in Figure 3, where

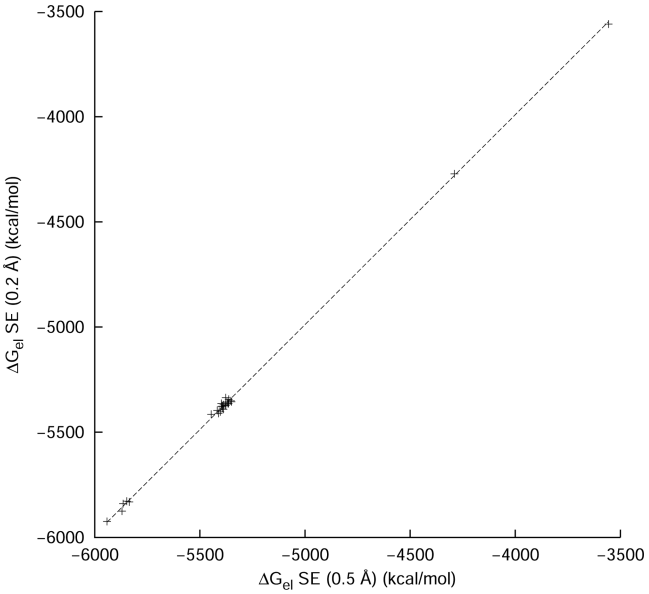


**Figure 3.** Electrostatic solvation energy, $\Delta G_{el}$, for all DNA-drug complexes computed with a solvent-excluded, SE, surface with a finest grid spacing of 0.5 Å plotted against the same energy computed with a finest grid spacing of 0.2 Å. The best-fit line has a slope of 1.00 and an $R^2$ = 0.999.

$\Delta G_{el}$ for the DNA-drug complexes computed with 0.5 Å and 0.2 Å grid spacings based on the SE surface are compared. The linear fit through these results produces an $R^2$ = 0.999 and a slope of 1.00 confirming converged results at the 0.5 Å spacing. Similarly well-converged results are obtained for the other complexes and surface definitions. However, note that the $\Delta G_{el}$ vary over a range of thousands of kcal/mol whereas the $\Delta\Delta G_{el}$ are typically several orders of magnitude smaller. Thus, the adequacy of a 0.5 Å spacing for the evaluation of $\Delta\Delta G_{el}$ is not ensured and must be determined separately. Indeed, an analogous plot for $\langle\Delta\Delta G_{el}\rangle$, produces $R^2$ = 0.87, after a single outlier with $\langle\Delta\Delta G_{el}\rangle$ > 60 kcal/mol (pdbid: 360d) is excluded (this case predicts a $\langle\Delta\Delta G_{el}\rangle$ that is almost an order of magnitude larger than for all other complexes).

Table 1 displays $\langle\Delta\Delta G_{el}\rangle$ and $\sigma_{GP}$ for the molecules, surface definitions, and grid spacings used in this study. As expected, $\sigma_{GP}$ generally increases with finest grid spacing (Figure 4), but the rate of increase differs with surface definition. The Gaussian surface, for example, shows a much slower rate of increase and smaller values of $\sigma_{GP}$ than either the SE or vdW surfaces. For both the vdW and SE surfaces, $\sigma_{GP}$ can exceed 10 kcal/mol at a 0.5 Å spacing, while for the Gaussian surface it is always less than 0.7 kcal/mol. Therefore, with the vdW or SE surfaces a large number of samples would be required to guarantee a reasonable estimate of $\langle\Delta\Delta G_{el}\rangle$, either using MM-PBSA methods[12] or random grid positioning, as was done in the present study.

More concerning though is the trend in $\langle\Delta\Delta G_{el}\rangle$ apparent in the data for the SE and vdW surfaces. For these surfaces, $\langle\Delta\Delta G_{el}\rangle$ increases with grid spacing, by more than 100 kcal/mol for some complexes, and furthermore, the results at the largest grid spacings are not even correlated with those at the finest grid spacings. When $R^2$ is computed between $\langle\Delta\Delta G_{el}\rangle$ at 0.3 Å and those at 1 Å for the SE surface, the results are as follows: for the DNA-drug complexes, $R^2$ = 0.41, for the barnase-barstar complexes, $R^2$ = 0.61, and for the RNA-peptide complexes, $R^2$ = 0.62. For the vdW surface, the corresponding numbers are $R^2$ = 0.59, $R^2$ = 0.12, and $R^2$ = 0.40. Clearly, rank ordering these complexes by $\langle\Delta\Delta G_{el}\rangle$ with a grid spacing of 1 Å would produce misleading results. These problems are less pronounced on the Gaussian surface, where the corresponding numbers are $R^2$ = 0.98, $R^2$ = 1.0, and $R^2$ = 0.91. Note that, $\langle\Delta\Delta G_{el}\rangle$ may not even be converged with finest grid spacings of 0.3 Å, as can be seen from Figure 5, where $\Delta\Delta G_{el}$ is computed for the different surface definitions for the barnase-barstar complex (pdbid: 1b27) at very fine mesh spacings on all three surface definitions. As can be seen from Table 1 and Figure 5, although $\sigma_{GP}$ is very small on these fine grids, $\langle\Delta\Delta G_{el}\rangle$ is still changing at some of the finest grid spacings.

**Examining the Effect of Surface Definition on $\Delta\Delta G_{el}$.** One option for improving the convergence of estimates of $\Delta\Delta G_{el}$ by grid-based solvers of the PB equation is to use a more numerically tractable surface definition. As seen from Table 1, the Gaussian surface definition examined in the present study yielded generally smaller $\sigma_{GP}$ and produced $\langle\Delta\Delta G_{el}\rangle$ estimates that depended less on grid spacing than those produced by either the SE or vdW surfaces, indicating that the Gaussian surface may be such a numerically tractable surface. However, ultimately a surface definition should be selected because of its ability to match experimental data. To date no single surface definition appears to offer consistently superior agreement with different experimental data sets. While the SE surface is the most popular, some groups have advocated for either the Gaussian or vdW surface,[18,22−24] claiming that their predictions of $\Delta G_{el}$, $\Delta\Delta G_{el}$, or p$K_a$ are in better agreement with experimental results. The different surface definitions considered here give very different estimates of $\langle\Delta\Delta G_{el}\rangle$. The correlations between $\Delta\Delta G$el computed based on the SE surface and those computed with the vdW surface were not very strong for the complexes considered here. $R^2$ = 0.58, 0.72, and 0.45 for the DNA-drug, RNA-peptide and barnase-barstar complexes, respectively. Similarly, when the predictions of $\Delta\Delta G_{el}$ by the Gaussian surface are compared to those with

Table 1. Average Electrostatic Binding Free Energies, $\langle \Delta\Delta G_{el} \rangle$,[a] and Standard Deviations, $\sigma_{GP}$, for All of the Complexes Used in This Study and Based on Three Different Surface Definitions and Four Different Finest Grid Spacings

| | | 0.3 Å | | 0.4 Å | | 0.5 Å | | 0.75 Å | | 1 Å | |
|---|---|---|---|---|---|---|---|---|---|---|---|
| | complexes | $\langle \Delta\Delta G_{el} \rangle$ | $\sigma_{GP}$ | $\langle \Delta\Delta G_{el} \rangle$ | $\sigma_{GP}$ | $\langle \Delta\Delta G_{el} \rangle$ | $\sigma_{GP}$ | $\langle \Delta\Delta G_{el} \rangle$ | $\sigma_{GP}$ | $\langle \Delta\Delta G_{el} \rangle$ | $\sigma_{GP}$ |
| | | | | | SE | | | | | | |
| DNA-drug | 102d | 9.8 | 0.1 | 9.9 | 0.7 | 12.9 | 2.3 | 32.4 | 8.8 | 55.9 | 19.3 |
| | 109d | 3.1 | 0.1 | 3.6 | 0.6 | 5.3 | 4.3 | 18.5 | 9.1 | 43.0 | 14.6 |
| | 121d | 23.9 | 0.1 | 23.7 | 1.3 | 27.2 | 4.3 | 58.1 | 14.2 | 90.8 | 19.8 |
| | 127d | 29.7 | 0.2 | 29.3 | 1.4 | 32.9 | 4.7 | 52.9 | 16.0 | 85.3 | 18.8 |
| | 129d | 40.3 | 0.1 | 40.3 | 0.6 | 41.9 | 2.4 | 56.1 | 9.7 | 95.4 | 19.9 |
| | 166d | 15.1 | 0.1 | 15.0 | 0.9 | 15.3 | 1.5 | 25.1 | 6.3 | 51.0 | 10.9 |
| | 195d | 3.0 | 0.1 | 3.1 | 0.5 | 3.4 | 2.2 | 21.9 | 8.0 | 54.4 | 16.6 |
| | 1d30 | 11.0 | 0.1 | 11.5 | 0.7 | 12.7 | 2.7 | 29.4 | 11.0 | 69.6 | 23.4 |
| | 1d63 | 12.9 | 0.1 | 12.7 | 1.1 | 15.3 | 3.7 | 47.1 | 20.4 | 71.1 | 19.3 |
| | 1d64 | 14.9 | 0.1 | 15.2 | 0.2 | 14.8 | 1.2 | 23.8 | 5.2 | 52.5 | 17.7 |
| | 1d86 | 25.2 | 0.1 | 25.4 | 1.2 | 30.9 | 4.3 | 71.0 | 17.8 | 115.1 | 28.1 |
| | 1dne | 21.9 | 0.1 | 21.4 | 2.3 | 26.5 | 4.3 | 57.5 | 9.8 | 99.0 | 13.7 |
| | 1eel | 15.6 | 0.2 | 15.6 | 1.5 | 18.7 | 5.2 | 43.2 | 18.1 | 79.3 | 24.7 |
| | 1fmq | 14.7 | 0.1 | 14.8 | 0.8 | 16.7 | 2.0 | 42.0 | 15.7 | 63.9 | 17.8 |
| | 1fms | 26.0 | 0.1 | 26.2 | 0.5 | 27.0 | 2.0 | 45.2 | 11.5 | 72.1 | 17.9 |
| | 1jtl | 11.5 | 0.2 | 11.6 | 1.0 | 15.2 | 4.7 | 32.8 | 12.9 | 86.0 | 34.6 |
| | 1lex | 11.0 | 0.2 | 11.3 | 1.1 | 16.2 | 4.0 | 49.1 | 9.6 | 87.8 | 29.2 |
| | 1prp | 11.7 | 0.1 | 11.6 | 0.8 | 12.2 | 1.5 | 24.7 | 10.3 | 48.5 | 18.0 |
| | 227d | 6.5 | 0.2 | 6.6 | 1.2 | 11.3 | 5.4 | 41.1 | 13.4 | 71.7 | 34.5 |
| | 261d | 3.3 | 0.2 | 3.7 | 1.4 | 9.1 | 3.4 | 37.7 | 13.4 | 79.7 | 24.1 |
| | 264d | 31.7 | 0.1 | 32.1 | 1.0 | 34.7 | 3.1 | 54.0 | 10.2 | 79.9 | 20.0 |
| | 289d | 16.8 | 0.1 | 16.7 | 1.8 | 18.2 | 4.4 | 49.0 | 18.2 | 72.2 | 18.3 |
| | 298d | 15.5 | 0.1 | 15.4 | 0.6 | 17.6 | 4.5 | 38.2 | 8.6 | 71.8 | 21.5 |
| | 2dbe | 5.5 | 0.1 | 5.5 | 0.5 | 7.1 | 2.6 | 24.6 | 12.7 | 59.4 | 18.7 |
| | 302d | 24.9 | 0.2 | 25.7 | 1.3 | 29.3 | 6.6 | 58.2 | 12.6 | 81.3 | 17.2 |
| | 311d | 10.3 | 0.2 | 9.8 | 2.7 | 13.5 | 6.1 | 42.5 | 13.8 | 80.7 | 28.0 |
| | 328d | 19.1 | 0.1 | 19.1 | 0.3 | 18.7 | 1.4 | 26.0 | 3.7 | 58.6 | 15.2 |
| | 360d | 55.5 | 0.1 | 55.6 | 1.6 | 57.2 | 3.0 | 82.3 | 18.0 | 109.8 | 19.7 |
| Barnase-Barstar | 1b27 | 85.9 | 0.2 | 86.2 | 2.2 | 96.7 | 4.8 | 172.9 | 24.1 | 273.8 | 46.4 |
| | 1b2s | 72.5 | 0.2 | 72.0 | 2.0 | 81.8 | 6.2 | 145.2 | 20.0 | 221.7 | 49.2 |
| | 1b2u | 78.9 | 0.2 | 79.0 | 1.9 | 87.4 | 5.5 | 146.2 | 17.4 | 199.8 | 36.2 |
| | 1b3s | 49.8 | 0.2 | 49.5 | 1.7 | 59.0 | 7.7 | 120.0 | 16.3 | 223.4 | 28.2 |
| | 1x1u | 75.6 | 0.3 | 75.8 | 2.3 | 85.9 | 6.0 | 167.9 | 24.7 | 257.8 | 26.5 |
| | 1x1w | 93.7 | 0.3 | 93.9 | 1.5 | 106.1 | 7.0 | 181.6 | 29.1 | 287.9 | 40.7 |
| | 1x1x | 117.8 | 0.4 | 118.2 | 2.9 | 133.5 | 9.1 | 214.1 | 31.5 | 309.2 | 41.9 |
| | 1x1y | 88.8 | 0.2 | 88.9 | 2.5 | 102.0 | 8.5 | 187.6 | 20.3 | 271.7 | 33.2 |
| | 2za4 | 75.6 | 0.3 | 76.1 | 2.3 | 85.2 | 6.7 | 135.7 | 25.9 | 222.5 | 40.4 |
| RNA-peptide | 1a1t | 114.9 | 0.3 | 115.2 | 3.2 | 131.3 | 6.7 | 237.5 | 21.3 | 351.1 | 47.2 |
| | 1a4t | 136.3 | 0.2 | 136.2 | 2.3 | 148.4 | 7.3 | 255.2 | 32.2 | 338.0 | 38.3 |
| | 1biv | 137.2 | 0.4 | 138.1 | 5.1 | 162.2 | 15.1 | 337.1 | 40.8 | 468.7 | 46.5 |
| | 1exy | 249.3 | 0.5 | 251.2 | 3.9 | 276.0 | 7.6 | 416.7 | 45.6 | 565.8 | 46.2 |
| | 1g70 | 174.2 | 0.3 | 173.2 | 3.2 | 193.5 | 8.8 | 292.0 | 19.1 | 390.9 | 43.0 |
| | 1hji | 61.1 | 0.2 | 60.5 | 2.1 | 69.6 | 5.6 | 120.3 | 26.2 | 181.5 | 34.8 |
| | 1i9f | 18.3 | 0.3 | 19.5 | 3.6 | 43.9 | 7.3 | 172.8 | 32.8 | 255.8 | 39.2 |
| | 1mnb | 171.3 | 0.4 | 171.1 | 2.7 | 193.4 | 10.7 | 305.4 | 46.3 | 420.2 | 47.9 |
| | 1nyb | 35.4 | 0.2 | 35.3 | 2.1 | 47.9 | 12.4 | 124.5 | 28.8 | 228.9 | 30.9 |
| | 1qfq | 56.3 | 0.4 | 56.4 | 2.7 | 72.0 | 16.9 | 136.4 | 37.6 | 239.0 | 46.0 |
| | 1ull | 84.4 | 0.3 | 82.5 | 4.4 | 118.8 | 11.5 | 319.0 | 59.3 | 516.5 | 60.4 |
| | 1zbn | 297.9 | 0.3 | 298.3 | 2.4 | 318.2 | 11.1 | 439.2 | 35.6 | 572.5 | 37.3 |
| | 2a9x | 414.0 | 0.2 | 414.3 | 1.4 | 421.5 | 5.0 | 480.0 | 31.7 | 551.9 | 27.8 |
| | 484d | 232.3 | 0.3 | 232.6 | 2.5 | 254.6 | 8.1 | 423.6 | 38.8 | 635.2 | 74.3 |
| | | | | | vdW | | | | | | |
| DNA-drug | 102d | −5.8 | 0.1 | −5.0 | 0.3 | −2.7 | 1.3 | 6.9 | 5.3 | 15.8 | 6.2 |
| | 109d | −4.5 | 0.1 | −3.6 | 0.4 | −1.7 | 1.5 | 9.5 | 7.8 | 32.1 | 13.4 |
| | 121d | 1.1 | 0.2 | 2.6 | 0.6 | 4.6 | 2.3 | 24.3 | 10.7 | 45.3 | 16.4 |
| | 127d | 0.6 | 0.1 | 1.6 | 0.7 | 4.1 | 2.1 | 16.4 | 10.3 | 37.0 | 17.2 |
| | 129d | 4.3 | 0.3 | 5.8 | 0.5 | 8.7 | 2.3 | 19.2 | 8.5 | 37.3 | 13.3 |


dx.doi.org/10.1021/ct300765w | J. Chem. Theory Comput. 2013, 9, 3677−3685

**Table 1. continued**

| | | 0.3 Å | | 0.4 Å | | 0.5 Å | | 0.75 Å | | 1 Å | |
|---|---|---|---|---|---|---|---|---|---|---|---|
| | complexes | $\langle\Delta\Delta G_{el}\rangle$ | $\sigma_{GP}$ | $\langle\Delta\Delta G_{el}\rangle$ | $\sigma_{GP}$ | $\langle\Delta\Delta G_{el}\rangle$ | $\sigma_{GP}$ | $\langle\Delta\Delta G_{el}\rangle$ | $\sigma_{GP}$ | $\langle\Delta\Delta G_{el}\rangle$ | $\sigma_{GP}$ |
| | | | | | vdW | | | | | | |
| | 166d | −2.8 | 0.1 | −2.1 | 0.9 | 0.6 | 2.3 | 5.4 | 4.4 | 23.4 | 8.5 |
| | 195d | −8.5 | 0.2 | −7.8 | 0.8 | −6.7 | 3.4 | 9.4 | 9.0 | 27.3 | 10.8 |
| | 1d30 | −1.1 | 0.2 | −0.1 | 0.6 | 1.5 | 2.2 | 10.2 | 5.9 | 31.1 | 12.7 |
| | 1d63 | −4.0 | 0.1 | −3.1 | 0.6 | −2.1 | 2.2 | 15.9 | 10.7 | 40.0 | 18.3 |
| | 1d64 | 0.2 | 0.1 | 0.9 | 0.4 | 1.9 | 1.4 | 6.6 | 3.6 | 20.0 | 8.1 |
| | 1d86 | −7.8 | 0.1 | −7.1 | 1.2 | −4.5 | 3.1 | 11.0 | 6.6 | 41.3 | 18.1 |
| | 1dne | −3.4 | 0.2 | −2.0 | 1.5 | 2.4 | 3.2 | 26.5 | 12.1 | 62.2 | 16.9 |
| | 1eel | −3.5 | 0.2 | −2.9 | 1.5 | 0.3 | 5.3 | 18.9 | 17.4 | 46.6 | 26.8 |
| | 1fmq | −3.9 | 0.2 | −3.1 | 0.8 | −0.5 | 3.0 | 16.5 | 15.0 | 30.2 | 18.6 |
| | 1fms | 0.8 | 0.3 | 1.9 | 0.6 | 3.4 | 1.9 | 14.7 | 5.3 | 27.5 | 10.7 |
| | 1jtl | −4.9 | 0.1 | −4.0 | 1.0 | 0.9 | 3.1 | 19.7 | 9.8 | 54.6 | 18.2 |
| | 1lex | −6.8 | 0.1 | −5.4 | 0.8 | −1.5 | 2.7 | 20.3 | 8.8 | 49.7 | 19.2 |
| | 1prp | −1.7 | 0.1 | −0.9 | 0.2 | 0.1 | 0.5 | 6.1 | 3.9 | 19.3 | 8.0 |
| | 227d | −5.3 | 0.3 | −5.1 | 1.4 | 0.1 | 5.6 | 18.3 | 8.8 | 31.8 | 16.5 |
| | 261d | −7.5 | 0.1 | −6.7 | 1.3 | −2.9 | 2.6 | 17.4 | 9.5 | 51.1 | 14.3 |
| | 264d | 4.7 | 0.2 | 6.1 | 0.7 | 8.8 | 1.5 | 23.1 | 7.9 | 44.9 | 15.4 |
| | 289d | −3.3 | 0.2 | −2.9 | 1.8 | −0.2 | 4.0 | 21.3 | 19.9 | 32.9 | 24.0 |
| | 298d | −2.3 | 0.2 | −1.5 | 0.8 | 0.9 | 3.3 | 16.0 | 9.4 | 38.3 | 22.8 |
| | 2dbe | −5.7 | 0.2 | −5.3 | 0.7 | −3.7 | 2.8 | 8.3 | 9.4 | 24.1 | 14.8 |
| | 302d | −0.7 | 0.1 | 0.6 | 0.4 | 2.3 | 1.7 | 14.9 | 6.1 | 33.7 | 9.1 |
| | 311d | −2.9 | 0.2 | −2.3 | 0.8 | −0.6 | 2.7 | 17.3 | 9.6 | 49.6 | 19.8 |
| | 328d | −1.8 | 0.1 | −1.1 | 0.2 | −0.2 | 0.2 | 2.5 | 1.2 | 15.4 | 5.0 |
| | 360d | 61.4 | 0.2 | 61.6 | 1.7 | 65.2 | 3.7 | 96.6 | 20.2 | 121.3 | 24.4 |
| Barnase-Barstar | 1b27 | −0.3 | 0.3 | 2.0 | 1.9 | 13.1 | 6.6 | 79.3 | 26.7 | 142.1 | 29.7 |
| | 1b2s | 7.7 | 0.3 | 9.6 | 2.3 | 23.2 | 6.4 | 91.1 | 18.3 | 140.6 | 34.3 |
| | 1b2u | 13.9 | 0.2 | 15.4 | 1.9 | 25.5 | 5.3 | 77.3 | 17.2 | 126.6 | 33.0 |
| | 1b3s | −19.3 | 0.2 | −17.8 | 1.5 | −8.4 | 4.5 | 48.3 | 18.9 | 108.7 | 25.4 |
| | 1x1u | −9.8 | 0.4 | −8.9 | 2.7 | 3.6 | 6.2 | 61.6 | 17.5 | 128.0 | 33.4 |
| | 1x1w | 3.2 | 0.3 | 6.1 | 1.5 | 17.8 | 6.5 | 81.8 | 25.2 | 151.8 | 33.2 |
| | 1x1x | 16.0 | 0.4 | 18.4 | 1.8 | 27.3 | 4.2 | 90.9 | 21.5 | 152.2 | 46.9 |
| | 1x1y | 1.3 | 0.4 | 3.3 | 1.7 | 14.2 | 7.3 | 77.3 | 24.4 | 121.8 | 26.1 |
| | 2za4 | 10.0 | 0.3 | 12.1 | 1.4 | 17.8 | 5.8 | 53.1 | 24.7 | 100.3 | 26.6 |
| RNA-peptide | 1a1t | 8.3 | 0.4 | 10.8 | 2.2 | 23.6 | 6.1 | 85.4 | 20.4 | 167.1 | 22.0 |
| | 1a4t | −0.1 | 0.2 | 3.6 | 1.2 | 10.1 | 3.5 | 67.2 | 18.9 | 138.2 | 34.3 |
| | 1biv | −3.2 | 0.5 | 3.1 | 3.3 | 21.9 | 12.0 | 159.3 | 36.0 | 282.5 | 68.7 |
| | 1exy | 35.5 | 0.6 | 41.9 | 2.0 | 57.2 | 7.3 | 146.6 | 24.7 | 234.1 | 47.2 |
| | 1g70 | 3.8 | 0.2 | 7.3 | 0.6 | 11.6 | 1.7 | 32.2 | 8.1 | 123.5 | 52.2 |
| | 1hji | −9.1 | 0.2 | −8.2 | 0.9 | −3.9 | 2.9 | 21.3 | 13.7 | 50.9 | 22.2 |
| | 1i9f | −42.3 | 0.3 | −39.6 | 3.0 | −24.5 | 5.3 | 59.6 | 27.1 | 139.5 | 41.4 |
| | 1mnb | 8.2 | 0.3 | 14.4 | 2.1 | 25.0 | 4.0 | 78.8 | 19.8 | 162.2 | 26.3 |
| | 1nyb | −21.0 | 0.4 | −20.0 | 2.0 | −8.9 | 8.8 | 41.5 | 28.4 | 114.3 | 28.3 |
| | 1qfq | −6.1 | 0.4 | −4.2 | 2.3 | 8.5 | 12.8 | 66.8 | 28.4 | 155.0 | 49.8 |
| | 1ull | −69.3 | 0.5 | −65.5 | 2.9 | −39.1 | 9.4 | 122.3 | 53.6 | 323.3 | 56.3 |
| | 1zbn | 84.7 | 1.1 | 93.5 | 3.3 | 108.4 | 4.2 | 175.2 | 26.7 | 276.0 | 34.8 |
| | 2a9x | 329.2 | 0.4 | 331.9 | 1.5 | 337.6 | 4.7 | 373.7 | 22.8 | 439.7 | 30.0 |
| | 484d | 15.6 | 0.7 | 21.8 | 3.3 | 42.5 | 7.2 | 145.0 | 33.0 | 304.6 | 59.5 |
| | | | | | Gaussian | | | | | | |
| DNA-drug | 102d | −52.0 | 0.0 | −52.3 | 0.1 | −52.5 | 0.1 | −53.8 | 0.5 | −51.7 | 4.0 |
| | 109d | −59.3 | 0.0 | −59.4 | 0.0 | −59.6 | 0.1 | −60.1 | 0.3 | −60.4 | 1.2 |
| | 121d | −56.3 | 0.1 | −56.4 | 0.1 | −56.4 | 0.1 | −57.5 | 0.6 | −53.5 | 3.9 |
| | 127d | −20.5 | 0.0 | −20.6 | 0.1 | −20.5 | 0.2 | −21.3 | 0.7 | −20.5 | 2.1 |
| | 129d | −16.0 | 0.0 | −16.2 | 0.0 | −16.2 | 0.1 | −16.9 | 0.2 | −17.2 | 0.8 |
| | 166d | −43.2 | 0.0 | −43.4 | 0.1 | −43.5 | 0.1 | −44.7 | 0.6 | −42.0 | 2.1 |
| | 195d | −68.1 | 0.0 | −68.2 | 0.0 | −68.4 | 0.1 | −69.4 | 0.5 | −65.2 | 2.5 |
| | 1d30 | −49.8 | 0.0 | −50.0 | 0.0 | −50.3 | 0.1 | −51.8 | 1.4 | −46.2 | 5.2 |
| | 1d63 | −50.8 | 0.0 | −51.1 | 0.0 | −51.4 | 0.1 | −53.0 | 1.5 | −45.9 | 5.4 |
| | 1d64 | −43.4 | 0.0 | −43.5 | 0.1 | −43.6 | 0.2 | −44.5 | 0.6 | −40.5 | 3.0 |
| | 1d86 | −58.3 | 0.1 | −58.6 | 0.1 | −58.8 | 0.1 | −59.8 | 0.8 | −55.2 | 3.3 |


dx.doi.org/10.1021/ct300765w | J. Chem. Theory Comput. 2013, 9, 3677−3685

**Table 1. continued**

| | | 0.3 Å | | 0.4 Å | | 0.5 Å | | 0.75 Å | | 1 Å | |
|---|---|---|---|---|---|---|---|---|---|---|---|
| | complexes | $\langle\Delta\Delta G_{el}\rangle$ | $\sigma_{GP}$ | $\langle\Delta\Delta G_{el}\rangle$ | $\sigma_{GP}$ | $\langle\Delta\Delta G_{el}\rangle$ | $\sigma_{GP}$ | $\langle\Delta\Delta G_{el}\rangle$ | $\sigma_{GP}$ | $\langle\Delta\Delta G_{el}\rangle$ | $\sigma_{GP}$ |
| | | | | | Gaussian | | | | | | |
| | 1dne | −71.2 | 0.1 | −71.5 | 0.1 | −71.7 | 0.1 | −73.0 | 0.8 | −68.9 | 2.5 |
| | 1eel | −54.9 | 0.0 | −55.2 | 0.0 | −55.4 | 0.1 | −56.2 | 0.3 | −56.9 | 1.7 |
| | 1fmq | −53.3 | 0.0 | −53.6 | 0.0 | −53.8 | 0.1 | −54.4 | 0.2 | −55.0 | 1.4 |
| | 1fms | −47.7 | 0.0 | −48.0 | 0.0 | −48.2 | 0.1 | −49.1 | 0.3 | −50.2 | 2.4 |
| | 1jtl | −44.5 | 0.0 | −44.6 | 0.1 | −44.7 | 0.1 | −45.3 | 0.9 | −42.4 | 4.5 |
| | 1lex | −74.3 | 0.0 | −74.6 | 0.0 | −74.7 | 0.1 | −75.8 | 0.9 | −68.9 | 5.4 |
| | 1prp | −45.4 | 0.0 | −45.6 | 0.0 | −45.7 | 0.1 | −46.7 | 0.7 | −44.3 | 2.1 |
| | 227d | −49.8 | 0.0 | −50.1 | 0.0 | −50.1 | 0.1 | −51.8 | 1.8 | −44.8 | 5.1 |
| | 261d | −86.9 | 0.0 | −87.1 | 0.0 | −87.3 | 0.1 | −88.1 | 1.0 | −82.2 | 3.0 |
| | 264d | −26.3 | 0.0 | −26.4 | 0.0 | −26.4 | 0.1 | −27.0 | 0.3 | −27.6 | 1.7 |
| | 289d | −53.0 | 0.0 | −53.3 | 0.0 | −53.5 | 0.0 | −54.3 | 0.2 | −54.2 | 2.3 |
| | 298d | −47.0 | 0.0 | −47.1 | 0.0 | −47.3 | 0.0 | −48.3 | 0.2 | −49.0 | 2.0 |
| | 2dbe | −52.4 | 0.0 | −52.6 | 0.0 | −52.8 | 0.1 | −54.1 | 1.4 | −50.0 | 6.0 |
| | 302d | −31.4 | 0.1 | −31.5 | 0.1 | −31.5 | 0.1 | −32.3 | 0.4 | −30.8 | 2.0 |
| | 311d | −68.6 | 0.3 | −68.3 | 0.0 | −68.6 | 0.2 | −69.7 | 0.9 | −62.0 | 6.5 |
| | 328d | −39.5 | 0.0 | −39.6 | 0.0 | −39.8 | 0.1 | −40.5 | 0.4 | −41.0 | 1.2 |
| | 360d | −11.2 | 0.0 | −11.4 | 0.0 | −11.6 | 0.0 | −12.4 | 0.3 | −13.2 | 1.5 |
| Barnase-Barstar | 1b27 | −78.9 | 0.1 | −79.2 | 0.1 | −79.6 | 0.1 | −81.2 | 1.3 | −75.0 | 4.5 |
| | 1b2s | −52.6 | 0.0 | −52.6 | 0.1 | −52.9 | 0.1 | −53.9 | 1.3 | −48.0 | 3.3 |
| | 1b2u | −36.7 | 0.1 | −36.8 | 0.1 | −37.2 | 0.2 | −38.7 | 1.6 | −33.3 | 6.1 |
| | 1b3s | −112.9 | 0.0 | −113.1 | 0.0 | −113.7 | 0.2 | −115.0 | 1.3 | −110.2 | 3.9 |
| | 1x1u | −108.4 | 0.1 | −108.8 | 0.1 | −109.4 | 0.1 | −110.9 | 1.1 | −105.1 | 5.9 |
| | 1x1w | −89.9 | 0.0 | −84.3 | 0.1 | −84.7 | 0.1 | −86.3 | 1.4 | −81.8 | 5.0 |
| | 1x1x | −42.1 | 0.1 | −42.3 | 0.1 | −42.8 | 0.2 | −44.5 | 1.6 | −37.9 | 5.0 |
| | 1x1y | −65.5 | 0.0 | −65.6 | 0.0 | −66.2 | 0.1 | −67.6 | 1.2 | −61.8 | 6.5 |
| | 2za4 | −39.4 | 0.1 | −39.6 | 0.1 | −39.9 | 0.1 | −40.8 | 1.5 | −36.9 | 3.6 |
| RNA-peptide | 1a1t | −104.3 | 0.1 | −105.0 | 0.1 | −105.7 | 0.2 | −108.8 | 2.6 | −96.1 | 5.2 |
| | 1a4t | −140.1 | 0.2 | −140.8 | 0.2 | −141.7 | 0.2 | −144.8 | 3.1 | −124.8 | 9.3 |
| | 1biv | −267.4 | 0.1 | −268.3 | 0.1 | −269.6 | 0.2 | −273.5 | 3.0 | −256.5 | 10.2 |
| | 1exy | −105.5 | 0.1 | −106.8 | 0.2 | −107.7 | 0.2 | −112.4 | 3.0 | −93.3 | 8.4 |
| | 1g70 | −63.1 | 0.1 | −63.6 | 0.1 | −64.3 | 0.2 | −67.9 | 1.1 | −58.5 | 7.7 |
| | 1hji | −76.0 | 0.1 | −76.6 | 0.1 | −77.2 | 0.6 | −79.7 | 1.3 | −68.3 | 6.5 |
| | 1i9f | −164.5 | 0.1 | −165.0 | 0.1 | −165.4 | 0.6 | −167.7 | 2.9 | −148.6 | 4.8 |
| | 1mnb | −88.4 | 0.1 | −88.6 | 0.1 | −89.4 | 0.2 | −92.8 | 2.1 | −76.8 | 8.8 |
| | 1nyb | −147.0 | 0.1 | −147.5 | 0.1 | −148.0 | 0.2 | −149.7 | 1.7 | −132.4 | 12.3 |
| | 1qfq | −173.3 | 0.1 | −173.4 | 0.1 | −174.1 | 0.2 | −176.3 | 2.0 | −169.5 | 9.8 |
| | 1ull | −508.9 | 0.1 | −509.9 | 0.2 | −511.8 | 0.3 | −518.8 | 2.0 | −498.9 | 9.2 |
| | 1zbn | −81.0 | 0.1 | −81.6 | 0.1 | −82.8 | 0.3 | −86.0 | 2.3 | −71.4 | 7.5 |
| | 2a9x | 245.5 | 0.1 | 245.0 | 0.1 | 244.5 | 0.1 | 242.4 | 1.7 | 245.7 | 7.1 |
| | 484d | −178.2 | 0.1 | −178.9 | 0.2 | −180.4 | 0.3 | −184.2 | 3.4 | −162.0 | 9.1 |

[a] In units of kcal/mol.

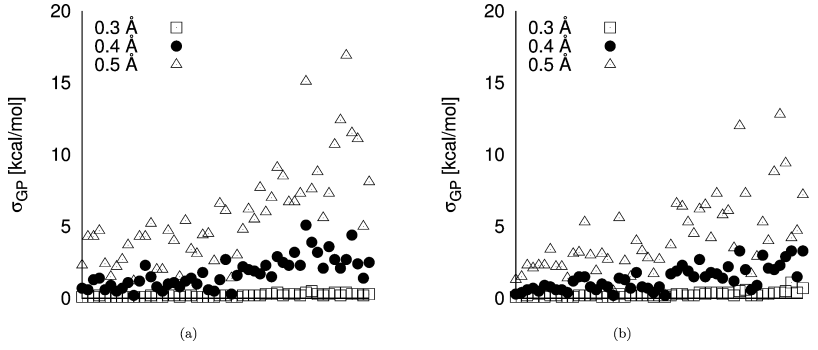


**Figure 4.** Standard deviations, $\sigma_{GP}$, of 30 different measurements of the electrostatic binding free energy, $\Delta\Delta G_{el}$, on randomly shifted grids at finest grid spacings of 0.3 Å, 0.4 Å, and 0.5 Å, as described in Methods. (a) The solvent-excluded surface. (b) The van der Waal's surface. No figure was made for the Gaussian surface because $\sigma_{GP}$ was too small to be represented on this scale, as can be seen from Table 1.


dx.doi.org/10.1021/ct300765w | J. Chem. Theory Comput. 2013, 9, 3677−3685

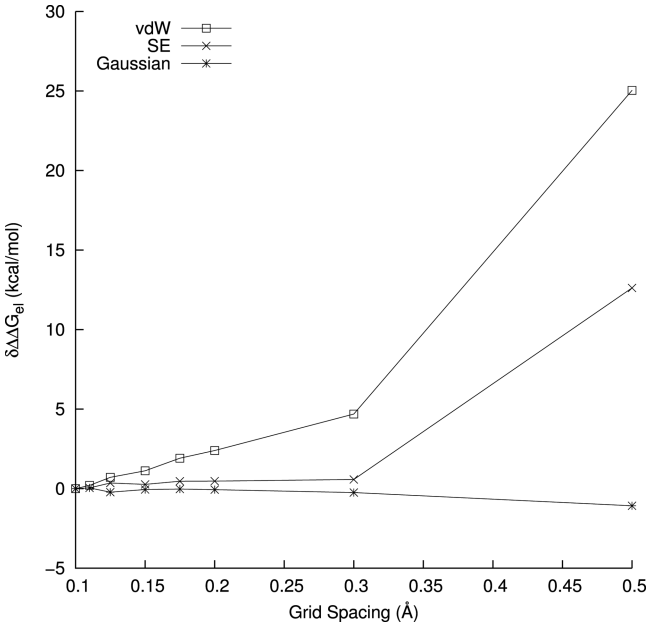


**Figure 5.** Difference, $\delta\Delta\Delta G_{el}$, between $\Delta\Delta G_{el}$ computed at a finest grid spacing of 0.1 and at larger grid spacings for the barnase-barstar complex (pdbid: 1b27) using the vdW, SE, and Gaussian ($\alpha$ =1.4) surface definitions.

the SE surface, $R^2$ = 0.56, 0.37, and 0.20 for the DNA-drug, RNA-peptide and barnase-barstar complexes, respectively. Consequently, the different surface definitions would yield very different rankings by $\langle\Delta\Delta G_{el}\rangle$. Additionally, the attractive numerical properties of the Gaussian surface will vanish at small $\alpha$ because in the limit of $\alpha$ = 0, the Gaussian surface will be identical to the vdW surface, which has much larger $\sigma_{GP}$ and $\langle\Delta\Delta G_{el}\rangle$ estimates that depend more on grid spacing.

## CONCLUSIONS

Estimates of $\Delta\Delta G_{el}$ from grid-based solvers of the PB equation inevitably contain numerical grid-discretization errors. Generally, the larger the grid spacing, the more sensitive is $\Delta\Delta G_{el}$ is to the placement of the grid. Eliminating this error at larger grid spacings requires either averaging over several PB calculations on slightly shifted grids or averaging over several related molecular-dynamics snapshots as is done in MM-PBSA. However, even when this averaging is performed, the resulting best estimate of $\Delta\Delta G_{el}$, $\langle\Delta\Delta G_{el}\rangle$, is also dependent on grid spacing. For the vdW and SE surfaces, errors in $\langle\Delta\Delta G_{el}\rangle$ at a grid spacing of 0.5 Å can exceed 30 kcal/mol, while a 1 Å grid spacing yields errors in excess of 100 kcal/mol. Additionally, because the systematic error in $\langle\Delta\Delta G_{el}\rangle$ at a particular grid spacing is very different for different complexes, ranking complexes by $\langle\Delta\Delta G_{el}\rangle$ yields varying rank orders at different grid spacings. Therefore users of grid-based solvers of the PB equation that attempt to rank complexes by $\langle\Delta\Delta G_{el}\rangle$, such as in structure-based drug-design studies, must be careful to assess and control this error. We advocate that calculations at different grid spacings should be performed to verify that PB predictions have converged with respect to grid spacing.

The data presented here indicate that the commonly used grid spacing of 0.5 Å may not be sufficiently fine to produce converged estimates of $\langle\Delta\Delta G_{el}\rangle$, at least for the vdW and SE surfaces, even though the predictions of $\Delta G_{el}$ appear to be well converged. Indeed, for some of the complexes, even a 0.3 Å grid appears inadequate for estimating $\langle\Delta\Delta G_{el}\rangle$ in some applications.

One option for circumventing these convergence issues in grid-based solvers of the PB equation is to employ a more numerically tractable molecular surface definition. The Results show that a Gaussian surface definition with adequate $\alpha$ achieves much faster convergence with grid spacing, as both $\sigma_{GP}$ and $\langle\Delta\Delta G_{el}\rangle$ converge much more rapidly than for either the vdW or SE surfaces. Presumably, this numerical stability is due to the elimination of the small crevices, reentrant edges, and cusps present in the SE and vdW surfaces. However, a suitable choice of surface definition must be able to match experimental data and, unfortunately, this aspect of surface selection has not been settled in the literature[24,25] and is not addressed in the present study. As shown in the Results, the predictions of $\langle\Delta\Delta G_{el}\rangle$ produced by different surface definitions are very different. While determining an optimal surface definition remains a challenging problem, the results developed here underscore the importance of establishing convergence and selecting adequate grid size as prerequisites in any attempt to find such a surface.

## AUTHOR INFORMATION

### Corresponding Author

*E-mail: mfenley@sb.fsu.edu. Phone: (850)644-7961. Fax: (850)644-7244.

### Notes

The authors declare no competing financial interest.

## ACKNOWLEDGMENTS

This publication was made possible by Grant GM5R44GM073391 from the National Institute of General Medical Sciences of the National Institute of Health. We would like to thank Mr. Travis Mackoy for his help in preparing some of the figures.

## REFERENCES

(1) Boschitsch, A. H.; Fenley, M. O. Hybrid boundary element and finite difference method for solving the nonlinear Poisson−Boltzmann equation. *J. Comput. Chem.* **2004**, *25*, 935−955.

(2) Boschitsch, A. H.; Fenley, M. O. A new outer boundary formulation and energy corrections for the nonlinear Poisson−Boltzmann equation. *J. Comput. Chem.* **2007**, *28*, 909−921.

(3) Boschitsch, A. H.; Fenley, M. O. A Fast and Robust Poisson−Boltzmann Solver Based on Adaptive Cartesian Grids. *J. Chem. Theory Comput.* **2011**, *7*, 1524−1540.

(4) Boschitsch, A. H.; Fenley, M. O.; Zhou, H.-X. Fast Boundary Element Method for the Linear Poisson−Boltzmann Equation. *J. Phys. Chem. B* **2002**, *106*, 2741−2754.

(5) Fenley, M. O.; Mascagni, M.; McClain, J.; Silalahi, A. R. J.; Simonov, N. A. Using Correlated Monte Carlo Sampling for Efficiently Solving the Linearized Poisson−Boltzmann Equation Over a Broad Range of Salt Concentration. *J. Chem. Theory Comput.* **2009**, *6*, 300−314.

(6) Simonov, N. A.; Mascagni, M.; Fenley, M. O. Monte Carlo-based linear Poisson-Boltzmann approach makes accurate salt-dependent solvation free energy predictions possible. *J. Chem. Phys.* **2007**, *127*, 185105−6.

(7) Mackoy, T.; Harris, R. C.; Johnson, J.; Mascagni, M.; Fenley, M. O. Numerical Optimization of a Walk-on-Spheres Solver for the Linear Poisson-Boltzmann Equation. *Commun. Comput. Phys.* **2013**, *13*, 195−206.

(8) Baginski, M.; Fogolari, F.; Briggs, J. M. Electrostatic and non-electrostatic contributions to the binding free energies of anthracycline antibiotics to DNA. *J. Mol. Biol.* **1997**, *274*, 253−267.

(9) Sharp, K. A. Electrostatic interactions in hirudin-thrombin binding. *Biophys. Chem.* **1996**, *61*, 37−49.
(10) Shivakumar, D.; Williams, J.; Wu, Y.; Damm, W.; Shelley, J.; Sherman, W. Prediction of Absolute Solvation Free Energies using Molecular Dynamics Free Energy Perturbation and the OPLS Force Field. *J. Chem. Theory Comput.* **2010**, *6*, 1509−1519.
(11) Nicholls, A.; Mobley, D. L.; Guthrie, J. P.; Chodera, J. D.; Bayly, C. I.; Cooper, M. D.; Pande, V. S. Predicting Small-Molecule Solvation Free Energies: An Informal Blind Test for Computational Chemistry. *J. Med. Chem.* **2008**, *51*, 769−779.
(12) Kollman, P. A.; Massova, I.; Reyes, C.; Kuhn, B.; Huo, S.; Chong, L.; Lee, M.; Lee, T.; Duan, Y.; Wang, W.; Donini, O.; Cieplak, P.; Srinivasan, J.; Case, D. A.; Cheatham, T. E. Calculating Structures and Free Energies of Complex Molecules: Combining Molecular Mechanics and Continuum Models. *Acc. Chem. Res.* **2000**, *33*, 889−897.
(13) Yu, Z.; Jacobson, M. P.; Friesner, R. A. What role do surfaces play in GB models? A new-generation of surface-generalized Born model based on a novel gaussian surface for biomolecules. *J. Comput. Chem.* **2006**, *27*, 72−89.
(14) Berman, H. M.; Westbrook, J.; Feng, Z.; Gilliland, G.; Bhat, T. N.; Weissig, H.; Shindyalov, I. N.; Bourne, P. E. The Protein Data Bank. *Nucleic Acids Res.* **2000**, *28*, 235−242.
(15) Fenley, M. O.; Harris, R. C.; Jayaram, B.; Boschitsch, A. H. Revisiting the Association of Cationic Groove-Binding Drugs to DNA Using a Poisson-Boltzmann Approach. *Biophys. J.* **2010**, *99*, 879−886.
(16) Dolinsky, T. J.; Nielsen, J. E.; McCammon, J. A.; Baker, N. A. PDB2PQR: an automated pipeline for the setup of Poisson−Boltzmann electrostatics calculations. *Nucleic Acids Res.* **2004**, *32*, W665−W667.
(17) Weiner, S. J.; Kollman, P. A.; Nguyen, D. T.; Case, D. A. An all atom force field for simulations of proteins and nucleic acids. *J. Comput. Chem.* **1986**, *7*, 230−252.
(18) Grant, J. A.; Pickup, B. T.; Nicholls, A. A smooth permittivity function for Poisson−Boltzmann solvation methods. *J. Comput. Chem.* **2001**, *22*, 608−640.
(19) Baker, N. A.; Sept, D.; Joseph, S.; Holst, M. J.; McCammon, J. A. Electrostatics of nanosystems: Application to microtubules and the ribosome. *Proc. Natl. Acad. Sci. U.S.A.* **2001**, *98*, 10037−10041.
(20) Feig, M.; Onufriev, A.; Lee, M. S.; Im, W.; Case, D. A.; Brooks, C. L. Performance comparison of generalized born and Poisson methods in the calculation of electrostatic solvation energies for protein structures. *J. Comput. Chem.* **2004**, *25*, 265−284.
(21) Reyes, C. M.; Kollman, P. A. Structure and thermodynamics of RNA-protein binding: using molecular dynamics and free energy analyses to calculate the free energies of binding and conformational change. *J. Mol. Biol.* **2000**, *297*, 1145−1158.
(22) Word, J. M.; Nicholls, A. Application of the Gaussian dielectric boundary in Zap to the prediction of protein pKa values. *Proteins* **2011**, *79*, 3400−3409.
(23) Dong, F.; Zhou, H.-X. Electrostatic contribution to the binding stability of protein−protein complexes. *Proteins* **2006**, *65*, 87−102.
(24) Pang, X.; Zhou, H.-X. Poisson-Boltzmann Calculations: van der Waals or Molecular Surface? *Commun. Comput. Phys.* **2013**, *13*, 1−12.
(25) Decherchi, S.; Colmenares, J.; Catalano, C. E.; Spagnuolo, M.; Alexov, E.; Rocchia, W. Between Algorithm and Model: Different Molecular Surface Definitions for the Poisson-Boltzmann Based Electrostatic Characterization of Biomolecules in Solution. *Commun. Comput. Phys.* **2013**, *13*, 61−89.